Two-dimensional infrared spectra of isotopically diluted amyloid fibrils from Aβ40

Yung Sam Kim[†], Liu Liu[‡], Paul H. Axelsen[‡§], and Robin M. Hochstrasser[†§]

[†]Department of Chemistry, University of Pennsylvania, Philadelphia, PA 19104-6323; and [‡]Departments of Pharmacology, Biochemistry and Biophysics, and Medicine/Infectious Diseases, University of Pennsylvania School of Medicine, Philadelphia, PA 19104-6084

Contributed by Robin M. Hochstrasser, March 26, 2008 (sent for review March 9, 2008)

The 2D IR spectra of the amide-I vibrations of amyloid fibrils from Aβ40 were obtained. The matured fibrils formed from strands having isotopic substitution by $^{13}C{=}{=}^{18}O$ at Gly-38, Gly-33, Gly-29, or Ala-21 show vibrational exciton spectra having reduced dimensionality. Indeed, linear chain excitons of amide units are seen, for which the interamide vibrational coupling is measured in fibrils grown from 50% and 5% mixtures of labeled and unlabeled strands. The data prove that the 1D excitons are formed from parallel in-register sheets. The coupling constants show that for each of the indicated residues the amide carbonyls in the chains are separated by 0.5 ± 0.05 nm. The isotope replacement of Gly-25 does not reveal linear excitons, consistent with the region of the strand having a different structure distribution. The vibrational frequencies of the amide-I modes, freed from effects of amide vibrational excitation exchange by 5% dilution experiments, point to there being a component of an electric field along the fibril axis that increases through the sequence Gly-38, Gly-33, Gly-29. The field is dominated by side chains of neighboring residues.

β-amyloid 40 | exciton | two-dimensional infrared spectroscopy

Amyloid fibrils are found in the brain tissue of persons with Alzheimer's disease, where they accumulate as plaques surrounded by regions of neuronal death. Although it remains unclear whether fibril formation is a cause of the neuronal loss in Alzheimer's disease, or a byproduct of another neurotoxic process, the formation and structure of amyloid fibrils is of intense interest.

Fibrils are composed primarily of β-amyloid (Aβ) proteins that range in length from 39 to 42 residues. They diffract x-rays with a characteristic "cross-β" pattern (1–3), indicating that the polypeptide strands lie transverse to the fibril axis, with an interstrand spacing that is typical of a β-sheet. Solid-state NMR (4) and EPR (5) studies have shown that the β-sheet configuration is parallel and in register. Based on information from NMR, supplemented with information from atomic force microscopy, electron microscopy, and cross-linking studies, Tycko and coworkers (6, 7) have developed detailed models of the fibrils formed by 40-residue (Aβ40) proteins. These models feature parallel in-register β-sheets involving residues 9–24 and 30–40 and a loop region, 23–29, that can vary with fibrillization conditions. A monofilament is formed by folding of each polypeptide chain such that the two sheets are apposed to each other, and two such monofilaments comprise the fibril (Fig. 1*A*). There is significant plasticity in the structural features of amyloid fibrils (8), and alternative models have been proposed (9).

In the current work the structure and internal dynamics of amyloid fibrils are examined by 2D IR spectroscopy (10–12). There has been a considerable amount of experimental work relating the 2D IR spectra of small peptide aggregates to their structure (13–17), and the recent experimental and theoretical applications of 2D IR have involved macromolecular systems such as folding proteins (18) and fibrils (19, 20).

Vibrational states within fibrils would be expected to resemble those of molecular crystals more so than small molecules or globular proteins. Accordingly, ideas introduced some time ago to investigate excitations in solids by means of isotope dilution or replacement (21) should be useful in characterizing amyloid fibrils. This approach is in contrast to isotope editing of smaller molecules where the goal is to isolate the spectra of individual group vibrations. Amide-I IR spectra of parallel β-sheets are dominated by motions in backbone C=O groups, but they are strongly influenced by intrastrand coupling and, to a lesser extent, interstrand coupling (14, 22–25). The coupling between the two apposing β-sheets of the fibril is expected to be relatively weak, rendering excitons in a β-sheet to be effectively delocalized in only two dimensions. Their spatial extent is limited by site energy fluctuations and static imperfections (26–29).

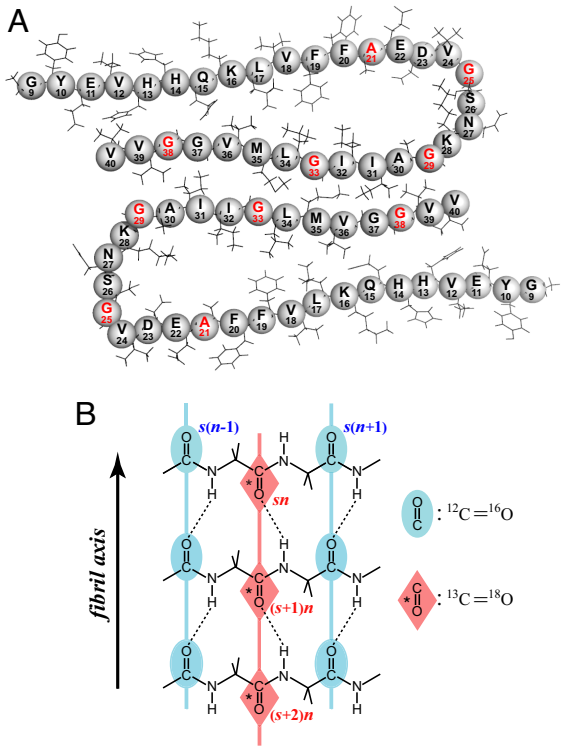

Fig. 1. Diagrams of Aβ40 fibrils. (*A*) A cross section of two laterally displaced molecular layers of the Aβ40 fibril according to Petkova *et al.* (6). Residues 9–40 are shown. (*B*) Idealized structure of a portion of the parallel β-sheet. The strands are indicated by *s*, and the residue number in a given strand is indicated by *n*. The asterisk denotes the carbonyl group of a $^{13}C{=}^{18}O$ doubly labeled amide group. Dotted lines represent hydrogen bonds.

Author contributions: P.H.A. and R.M.H. designed research; Y.S.K. and L.L. performed research; Y.S.K. analyzed data; and Y.S.K., P.H.A., and R.M.H. wrote the paper.

The authors declare no conflict of interest.

[§]To whom correspondence may be addressed. E-mail: axe@pharm.med.upenn.edu or hochstra@sas.upenn.edu

This article contains supporting information online at www.pnas.org/cgi/content/full/0802993105/DCSupplemental.

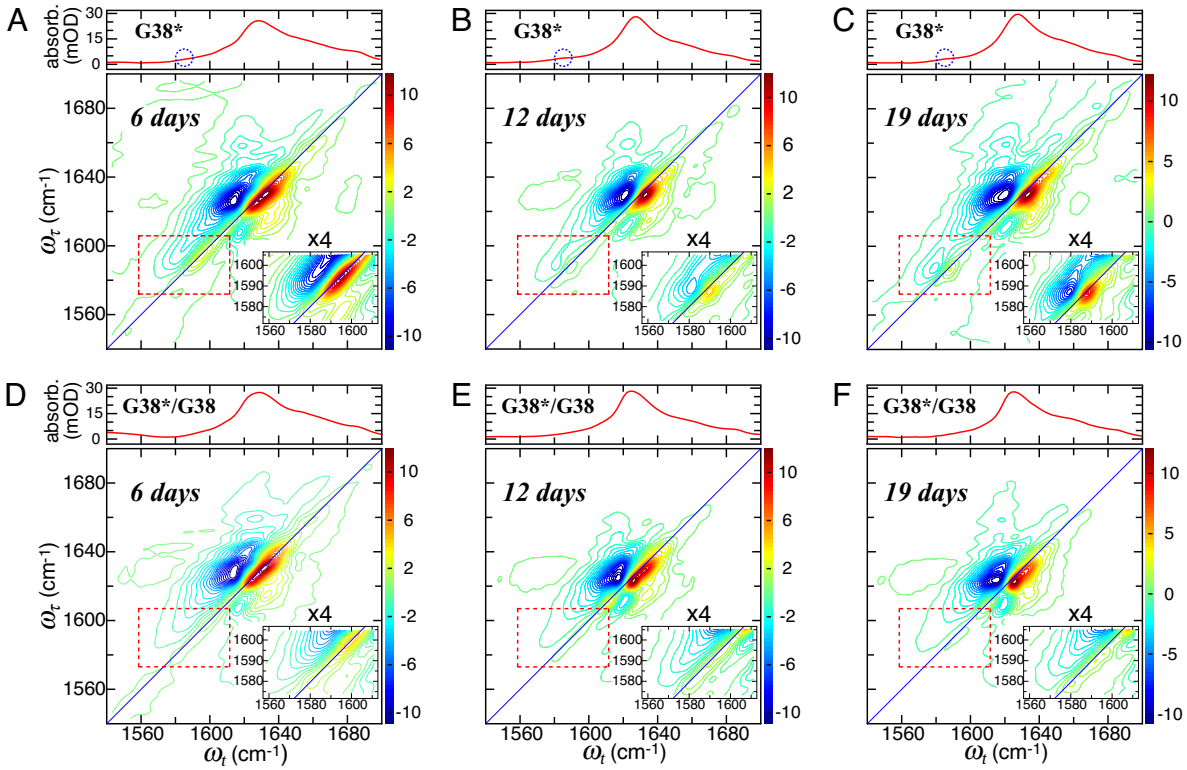

Fig. 2. Linear and 2D IR spectra of Aβ40 doubly labeled with $^{13}C{=}{=}^{18}O$ at Gly-38 (G38*) and a 1:1 mixture of G38* and unlabeled Aβ40 (G38*/G38) at different maturation times. (*A–C*) Linear IR spectra and 2D IR spectra at $T = 0$ of G38* at maturation times of 6 days (*A*), 12 days (*B*), and 19 days (*C*). (*D–F*) Linear IR spectra and 2D IR spectra at $T = 0$ of G38*/G38 at maturation times of 6 days (*D*), 12 days (*E*), and 19 days (*F*). The *Inset* in each 2D spectrum is an enlarged and four-times-intensified view of the area enclosed by the outlined region. The dotted circles in the linear spectra of *A–C* highlight the isotope-labeled amide-I transition regions. The magnitude of each 2D spectrum was scaled to have the same difference of maximum and minimum values.

The vibrational excitations can be radically altered when the atoms of an amide unit in an extended system are isotopically replaced. The energy shifts can result in the effective isolation of arrays having reduced dimensionality (21). When an amyloid fibril is formed from Aβ40 proteins in which one of the residues involved in a β-sheet has a single $^{13}C{=}{=}^{18}O$ substitution, the substituted groups form a linear array along the fibril axis (Fig. 1*B*). The substituted groups along this dimension have strong resonance coupling, whereas the interactions with unsubstituted groups are reduced by the ratio of the coupling magnitude to the isotope shift. Thus, the transport of vibrational excitations into the direction perpendicular to the fibril axis is greatly diminished, causing the vibrational exciton topology for the isotope region to be reduced to a nearly 1D situation. Under these conditions a quantitative analysis of the spectra–structure relationships can be obtained. The 2D IR spectra of amyloid fibrils with $^{13}C{=}{=}^{18}O$ substitutions exhibit novel manifestations of the extended 3D structure of the fibrils, including the spatial arrangement of the coupled amide units and the presence of both static and fluctuating electric fields.

Results

The formation of fibrils was compared at pD 7.4 and pD 2.0, and low pD was found to offer several significant advantages. One advantage was a much-reduced rate of fibril formation at the protein concentrations used, which permitted the examination of samples before they had formed fibrils. A second advantage was that fibril morphology at low pD much more closely resembled the long straight fibrils found in diseased brain tissue, including an ≈50-nm periodic narrowing that suggests the twisting of paired filaments (30, 31). [EM images are provided in supporting information (SI) Figs. S1 and S2.] At pD 7.4, the fibrils that formed were short and curvilinear. Fibrils formed at pD 7.4 also exhibited an additional absorbance band, attributed to amino acid side chains, that overlapped with that of $^{13}C{=}{=}^{18}O$. This absorbance could be recorded in a background spectrum and subtracted from the spectra of labeled proteins. However, its intensity was negligible at pD 2.0, and such manipulations were obviated.

FTIR and 2D IR spectra of fibrils formed from Aβ40 labeled with $^{13}C{=}{=}^{18}O$ at Gly-38 (G38*), and from a 1:1 mixture of labeled and unlabeled Aβ40 (G38*/G38), are shown in Fig. 2. The isotopomers G38*, G33*, and A21* of Aβ40 all yielded similar spectra, so only the spectra for G38* are illustrated. The six linear spectra each have a prominent peak with maximum at ≈1,625 cm^{-1}. At earlier maturation times, and in solutions before fibril formation, the maxima are in the region 1,645–1,650 cm^{-1} (data not shown) (32, 33). The reason for this shift in the linear IR spectra is presumed to be the transition to β-structure and fibril formation, and this inference is supported by the EM images of Aβ40 fibrils (see SI Figs. S1 and S2). The 1,625-cm^{-1} peaks for both G38* and G38*/G38 vary in width from day 6 to day 12: the widths (measured at two-thirds of the peak height) were 27.1 cm^{-1} (day 6) and 20.0 cm^{-1} (day 12) for G38* and 26.5 (day 6) and 20.9 cm^{-1} (day 12) for G38*/G38. This decrease in peak widths, evident from visual inspection of Fig. 2, indicates that a more homogeneous fibril is formed during this period. There was no further decrease in 1,625-cm^{-1} peak widths between days 12 and 70. Other than these small differences in peak widths, the FTIR spectra of G38* and G38*/G38 are extremely similar to each other at different maturation times (compare Fig. 2 *A–C* with *D–F*). Isotope editing of an amide

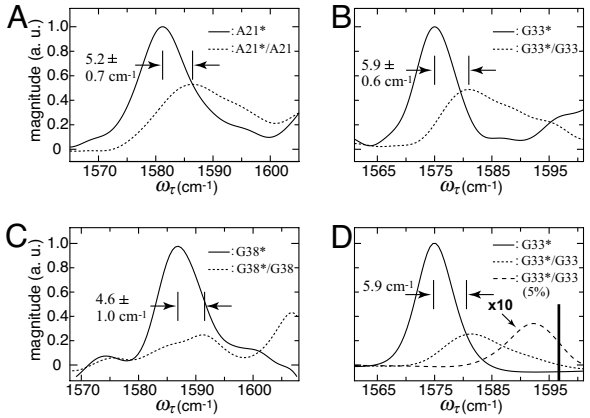

Fig. 3. Experimental and simulated traces of the Aβ40 fibril 2D IR spectra at $T = 0$. (*A–C*) Traces of the 2D IR signal along a line $\omega_t = \omega_\tau + 2$ cm^{-1} for A21* (solid) and A21*/A21 (dotted) (*A*), G33* (solid) and G33*/G33 (dotted) (*B*), and G38* (solid) and G38*/G38 (dotted) (*C*). (*D*) Simulated traces of the 2D IR spectra of fibrils formed from a 100% (solid), 50% (dotted), and 5% (dashed) G33-labeled peptide. The thick vertical line in *D* represents the frequency ν_o (defined in the text) of the isotope-labeled amide-I transition in the absence of any coupling. The coupling constant for the simulation of G33 (*D*) is $\alpha = -9.5$ cm^{-1}.

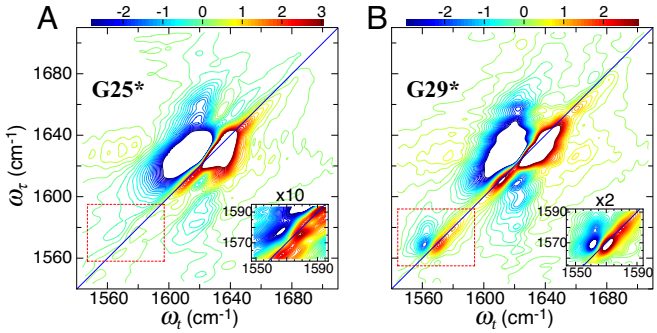

Fig. 4. 2D IR spectra of fibrils of G25* (^{13}C═^{18}O labeled at Gly-25) (*A*) and G29* (^{13}C═^{18}O labeled at Gly-29) (*B*) at $T = 0$ after 70 days of maturation. In each spectrum the white area corresponds to a flat top off-scale signal. The contours begin at 25% of the peak signals. The *Insets* are enlarged and 10-times-intensified (*A*) and two-times-intensified (*B*) views of the marked areas.

group with ^{13}C═^{18}O lowers the absorption frequency of that specific amide-I mode by ≈60 cm^{-1}. Peaks arising from these amide-I modes are just barely discernable in the linear spectra of G38* on days 12 and 19 (Fig. 2 *B* and *C*).

The 2D IR spectra of Fig. 2 display the 0–1 and 1–2 transitions of the amide modes in the (ω_τ, ω_t) plane. These transitions involve the fundamentals (shown in red in Fig. 2) and two-quantum regions (blue in Fig. 2) of the vibrational excitations. All of these spectra correspond to a waiting time of $T = 0$, where the effects of spectral diffusion and energy redistribution (see below) are not expected to be prominent. The six 2D IR spectra shown in Fig. 2 below their corresponding linear spectra clearly show that the amide-I transitions in the labeled amide groups of G38* evolve as maturation time increases. In each panel, the isotope transition spectral region is highlighted by a rectangle, and an expanded scale version is shown in the *Inset*. In Fig. 2 *B* and *C*, sharp peaks from fundamentals and excited-state transitions were observed at $\omega_\tau = 1{,}586.5$ cm^{-1}; they are split by 9 cm^{-1}, which is determined by the mode anharmonicity. In comparison, the ^{13}C═^{18}O transitions at 6 days (Fig. 2*A*) are red-shifted, broader, and weaker. The peaks at 1,625 cm^{-1} from unlabeled ^{12}C═^{16}O are considerably less sensitive to maturation.

The pronounced difference between the G38***** and G38*/G38 in the isotope region of the 2D IR spectra is seen in Fig. 2 *C Inset* and *F Inset*. The effect of dilution by 50% unlabeled peptide on the 2D IR spectra is shown in Fig. 3, which gives the traces of the 2D IR spectra of G38, G33, and A21 along a line $\omega_t = \omega_\tau + 2$ cm^{-1} close to the diagonals. The main result, common to all samples, is that the sharp isotope peak is no longer present in the 50% diluted sample: the spectrum becomes broader and is shifted to higher frequency. The shift between the lowest energy peak of the 50% isotopically diluted system and the neat fibril is 4.6 cm^{-1} for G38, 5.9 cm^{-1} for G33, and 5.2 cm^{-1} for A21: the error bars are noted in Fig. 3. On isotope dilution other bands appear at even higher frequency, closer to the ^{12}C═^{16}O bands, but they were partially obscured by overlap with these stronger transitions and so are not used in the analysis given here.

An experiment was also carried out on fibrils formed from G33 in which only 5% of the proteins contained isotope labels. The purpose was to locate the vibrational transition frequency of an isolated isotopically substituted amide group. The ^{13}C═^{18}O peak for the 5% sample of G33 was located at 1,594 cm^{-1}, which is shifted up in frequency by 19 cm^{-1} from the 100% G33* sample, whose peak signal is shown in Fig. 3*B*.

The spectra of G25* and G29* differed significantly from those of G38*, G33*, and A21*. The 2D IR signal for G29* showed two sharp bands separated by 12 cm^{-1} in the isotope region as shown in Fig. 4 *Insets*. On 50% isotope dilution of G29* the stronger component of the pair, which is at lower frequency, broadened and shifted by 6.3 cm^{-1}. There is a cross peak between these two bands in the 2D IR evidenced by the nearly vertical appearance of the 1–2 transition region, indicating that they represent modes that are coupled to one another. Fig. 4 also shows the G25* signal. The peak intensity of the G25* isotope band near 1,576 cm^{-1} falls much closer to the signal detection limit than in the other cases. The observed peak signal for G25* has only 12 ± 3% of the magnitude of the signals seen for the other isotopomers, suggesting that a different structure prevails in the region of this residue.

The sharp spectra of the fibrils enabled accurate measurement of the isotope-labeled residue peak positions for G38*, G33*, G29* (lower-frequency band), G25*, and A21*. The results were 1,586.5 (9.5) cm^{-1}, 1,575 (8.5) cm^{-1}, 1,568 (10.5) cm^{-1}, 1,576 (11.0) cm^{-1}, and 1,581 (10.5) cm^{-1}, respectively, where the 2D IR line widths are given in parentheses. The spectral shifts between the labeled amide-I modes of fibrils formed from different Aβ40 isotopomers are indicative of a heterogeneous structural environment for these residues.

The 2D IR data also exhibit cross peaks between the isotope-labeled residue and the main bands. For example, Fig. 4*A* for G25* shows a cross peak close to $\omega_t = 1{,}620$ cm^{-1} that stretches over a broad range of ω_τ. This result is consistent with there being a broad isotope peak in the 1,560- to 1,590 cm^{-1} region for G25* that is too weak to be seen above background. Such cross peaks were not present in unlabeled Aβ40. Very weak transitions, not seen in FTIR, can be exposed by their cross peaks with strong transitions in the 2D IR because the cross peak signal is approximately proportional to their geometric mean.

The 2D IR spectra at different waiting times for G38*, G33*, G29*, and A21* showed some dependence on waiting time (data not shown). In the case of G38* and G33* the changes were slight. However, for G29* and A21* significant evolution of the 2D IR spectral shapes in the neighborhood of the ^{13}C═^{18}O transition were seen. In both cases the diagonal peaks tilt toward the vertical and cross peaks develop as T increases into the picosecond regime, indicating that the transition frequencies are time-dependent and that energy redistribution is occurring on the time scale of the experiment. This article focuses entirely on

the $T = 0$ signals, before the occurrence of any of this relaxation, which is not considered further here.

Discussion

The results are explained by properties of amide-I modes associated with parallel β-sheets. In Fig. 1*B* the strands of an ideal β-sheet are labeled by s and the carbonyls on a strand are labeled by n. The coupling between the relevant H-bonded amide modes containing the sn and $(s \pm 1)n$ carbonyls in adjacent strands of a parallel sheet is generally agreed to be in the range of -9 to -11 cm^{-1}, while for the next-to-nearest neighbor strands sn and $(s \pm 2)n$ the coupling is -1 to -2 cm^{-1} (34). These results are consistent with a transition dipole–dipole interaction being important in the physical origin of the coupling. The couplings of nearest $s(n \pm 1)$ and next-to-nearest $s(n \pm 2)$ neighbors along the strand containing sn are in the range of $+0.5$–2.0 cm^{-1}. The isotope substitution decouples the transitions of the ^{13}C═^{18}O Glys from their neighbors except along the fibril axis, and linear chains are formed. The results are confirmatory of fibril structure models (6, 7), but the 2D IR spectra reveal heterogeneity in the frequencies and equilibrium dynamics.

Linear Chain Excitons. The spectra of perfect linear-chain vibrational excitons have qualitatively similar characteristics for nearest neighbor coupling and dipole–dipole interactions but can be best illustrated for the former case where the frequencies are $E_K/hc_o = \nu_K = \nu_o + 2a \cos K$ with $K = \pi k/(N + 1)$ and $k = 1$ to N. The coupling is denoted by α (cm^{-1}). The transition dipole moment squared from the vibrational ground state to the Kth state of the perfect lattice, μ_k^2, is dominated by the state with $k = 1$. When $N \gg 1$ this domination amounts to $>80\%$ (21, 35, 36). In that case the frequency-integrated absorption coefficient of the chain of N residues is $\approx 0.8N$ times that of a single amide unit. The photon echo signal varies as the fourth power of the transition dipole moment (37), so its peak signal scales approximately as N^2. The $k = 1$ state is the lowest-energy state of the linear band when the nearest neighbor coupling constant dominates and is negative. Therefore, the approximate linear chains created by isotope substitution at a strand residue are each expected to exhibit an intense, narrow vibrational transition in 2D IR that is shifted to lower frequency by $\approx 2\alpha$ from ν_o.

The transition to ν_o is seen at infinite isotope dilution when the spectrum consists of isolated ^{13}C═^{18}O molecules that do not resonantly couple to any neighboring amide groups. The most dilute system we have been able to examine is 5% ^{13}C═^{18}O in ^{12}C═^{16}O. The 5% spectrum should consist mainly of monomers at approximately $\nu_o - 2\alpha^2/\Delta\bar{\nu}_{iso}$, where $\Delta\bar{\nu}_{iso}$ (cm^{-1}) is the ^{13}C═^{18}O isotope shift. The situation is significantly altered when higher percentages of ^{13}C═^{18}O substitution are used. The relevant system then becomes a linear chain that is disordered by intermittent energy-mismatched sites.

The eigenstates, $|\lambda\rangle$ with energies E_λ, of a disordered linear chain are linear combinations $\Sigma_{k=1}^{N} c_{\lambda k}|k\rangle$ of the perfect aggregate excitons $|k\rangle$. These energies and wave functions depend on the microscopic disorder and the isotope doping. For $N \gg 1$ the spectrum of a particular disordered chain is approximately

$$S(E) = \sum_{\lambda=1}^{N} \left(\sum_{k=1}^{N} c_{\lambda k}\mu_k \right)^2 \delta(E - E_\lambda)$$

The spectrum of an ensemble for a particular doping level involves an average, $\langle S(E) \rangle$, over many disordered chains.

The eigenvalues of such a disordered chain were simulated by replacing a percentage of the diagonal elements of the exciton matrix by the ^{12}C═^{16}O vibrational transition at $\nu_o + 60$. The simulations were carried out on a model of the parallel β-sheet consisting of the isotopically replaced residue flanked by its neighbors (Fig. 1*B*). The non-nearest neighbor interactions along the chains and the nearest neighbor interactions across the chain fixed were fixed at -1.0 cm^{-1} and $+1.5$ cm^{-1}, respectively (34). Because of the isotope shift, the cross-chain coupling did not influence the simulated frequency shifts to any significant extent, thus verifying that the linear-chain spectral concept is robust. A Gaussian distribution of amide-I transition frequencies with a deviation of 4.0 cm^{-1} was introduced. Each transition was ascribed a population decay of 1.1 ps. and a 5.5-cm^{-1} homogeneous dephasing width. A Voigt profile line shape (37) was used for each amide unit. The simulated shifts of the transitions at different isotope dilutions were insensitive to the choices of these damping parameters, which mainly affected the relative intensities. The mean fraction of isotopically replaced residues on the chain was controlled numerically by constraints and random number generation. As an example, for the simulations of the fibrils grown from a 50% mixture of labeled and unlabeled strands we used 400 contracted strands with each having either one or zero isotope replacement. In the simulations the labeled strands were considered to have 92% isotopic purity of ^{13}C═^{18}O and 7% of ^{13}C═^{16}O (see *Materials and Methods*). The random number generation led to an average doping level of 0.5 ± 0.025. To obtain simulated spectra an average over $\approx$1,000 such disordered chains was performed. Finally, the linear-chain nearest neighbor coupling was varied to obtain the best agreement between the experimental traces along the 2D IR diagonals and the simulation. The main prediction of the effect of isotopic dilution of a linear chain exciton by 50% is a broadening and a shift of ≈ 5 cm^{-1} to higher frequency as the $k = 1$ amplitude becomes redistributed over a wider frequency range. There is also a drop in the cross section on dilution, which is larger than the number density effect of 50%.

The transition for the 5% sample of G33 at 1,594 cm^{-1}, which when compared with the 100% transition frequency yields $\alpha = -9.5$ cm^{-1}. The 5% peak is shifted from ν_o because of coupling of an isolated ^{13}C═^{18}O substituted residue with two nearest neighbor ^{12}C═^{16}O residues at 60 cm^{-1} to higher frequency. This down-shift can be visualized to reasonable accuracy from perturbation theory as $2\alpha^2/60 = 3.0$ cm^{-1}. The 5% simulation is also shown in Fig. 3*D*. The solid vertical line in that figure marks the transition frequency ν_o used in the simulation before any coupling is introduced. The ^{13}C═^{18}O isotope shift of 60 cm^{-1} is an estimate, but the results are not sensitive to $\pm 10\%$ changes in that quantity.

The observed linear-chain excitons must arise from parallel in-register β-sheets, and even without a quantitative analysis the isotopic dilution results of Fig. 3 are consistent with those for parallel sheets having an interstrand coupling in the range of -10 cm^{-1}. Similar results are seen for G33, G29, and A21. Fig. 3 shows the comparisons of the experimental and simulated 2D IR spectra at 50% dilution for G38*, G33*, G29*, and A21*. The ν_o values used for the simulations in Fig. 3*D* for G33 were 1,597 and 1,657 cm^{-1}, respectively, for ^{13}C═^{18}O and ^{12}C═^{16}O amide-I modes, with the former being measured from the 5% experiment and the latter having 60 cm^{-1} added to account for the isotope shift. By matching the 50% dilution shifts with simulations, linear-chain coupling constants were deduced as follows: -8.5 ± 1.6 cm^{-1} (A21), -10.0 ± 1.8 cm^{-1} (G29), -9.5 ± 1.6 cm^{-1} (G33), and -7.5 ± 2.3 cm^{-1} (G38). The 50% experiments yield values of the linear chain coupling that are within experimental error of those obtained from the difference between the band center ν_o, measured in the 5% experiment, and the bottom of the linear chain exciton band, measured in the 100% experiment.

The experimental shifts provided estimates of the interstack distances assuming a point dipole–dipole potential with the dipole of an amide group directed at 20° to the carbonyl groups (38) and in the plane of the sheets. The separations between the point dipoles were found to be 0.51 ± 0.04 nm (A21*), $0.48 \pm$

0.04 nm (G29*), 0.49 ± 0.03 nm (G33*), and 0.53 ± 0.06 nm (G38*). These results compare extremely well with results from NMR that indicated a 0.48 ± 0.05-nm repeat distance between the backbone carbonyl carbons in the parallel in-register regions of the fibrils (39). If the transition dipoles were tilted out of the plane of the sheet by as much as 20°, there would be a 7% decrease of the 2D IR predicted repeat distances based on 0° tilt. The small variations found in the coupling between stacks may reflect variations in this angle, but this remains as an open question.

Regions That Do Not Show Linear Chain Excitons. The results for G25* are quite different from those described above, so the presence of linear chains on isotope dilution of that region of the fibril is not indicated: a peak having ≈12% of the intensity of the other examples is observed. This indication is consistent with the NMR chemical shifts in the loop region of residues 25–29, which differ from those expected for a β-strand (6). The 2D IR signal for G29* showed two sharp bands in the isotope region (Fig. 4), and the stronger component at lower frequency displayed the broadening and shifting behavior already shown for G38*, G33*, and A21*. The presence of the two bands indicates that the structure of a fibril is not uniform in this region. The cross peaks between the two G29* bands indicate that both the vibrations are a property of each fibril. The 2D IR results suggest that two structural types are adopted in the G29 region and that the persistence length of one of them is sufficient to support linear-chain spectral characteristics.

Spectral Shifts. The variability of the spectral shifts of the amide-I modes for different residues reveals a structural and/or environmental heterogeneity of the fibrils. The analysis has shown clearly that the vibrational excitation exchange couplings are similar at each of the sites that were examined. Therefore, these large frequency variations of as much as 18 cm^{-1} are attributed to changes in ν_o. The shifts are suggested to be dominated by the variations of the electric field directed roughly along the carbonyl groups in the linear chains. Based on theoretical predictions of the importance of the electric field and its gradients in determining the amide-I mode frequency (40–43), the frequencies of isotopically substituted transitions in a β-hairpin were shown to be very sensitive to the field at the particular amide group (44) from other residues of the backbone and from the surrounding water molecules. In the present case the field may arise from partial charges of other residues, from side chains, and from included water and ions. It is expected that the frequency of the amide-I mode will decrease as the magnitude of the electric field along the carbonyl group increases; therefore, the component along the fibril axis must increase from G38* to G33* to G29* (lowest-frequency band). The field projection onto the in-register carbonyls on the other side of the bend at A21* is similar to that for G38*. These experimental features were consistent with estimates of the electric field based on the APBS software package for the numerical solution of the Poisson–Boltzmann equation, a continuum model for describing electrostatic interactions (45). The partial charges on the residues neighboring the linear chains, for example, the charged lysine neighboring G29*, are important. Both G38* and G33* have neighboring residues that have nonpolar side chains. The field differences between residues found in the simulation are ≈24 MV/cm, which are known (40–43) to cause shifts of ≈20 cm^{-1}, similar to those observed. A more complete computation will need to treat the influence of water molecules and ions that may be occluded in the fibril near the region between G29 and A21.

The excitations are delocalized over ≈15 residues based on computations of the participation ratio (27). This delocalization averages the inhomogeneous broadening and sharpens the spectra (17).

Conclusions

The 2D IR spectra of the fibrils from Aβ40 formed from strands with $^{13}C{=}{=}^{18}O$ at Gly-38, Gly-33, Gly-29, or Ala-21 show 1D exciton spectra that are formed by the isotope dilution of parallel in-register β-sheets. The couplings indicate a repeat distance of 0.5 ± 0.05 nm. The Gly-25 substitution does not reveal linear excitons, consistent with the loop region of the strand having a different structure distribution. The vibrational frequencies of the amide-I modes, freed from effects of excitation exchange, manifest an electric field along the fibril axis, which increases through the sequence Gly-38, Gly-33, Gly-29. The field is dominated by side chains of neighboring residues and may involve included water and ions.

Materials and Methods

Protein Synthesis. Aβ40 with the sequence DAEFRHDSGY EVHHQKLVFF AEDVGSNKGA IIGLMVGGVV was synthesized by using standard solid phase techniques and purified to ≥95% purity by reversed-phase HPLC at the Keck Biotechnology Resource Laboratory at Yale University (New Haven, CT). $^{13}C_1$-glycine, $^{13}C_1$-alanine, and ^{18}O-water were obtained from Cambridge Isotope Laboratories. The two ^{13}C-labeled amino acids underwent acid-catalyzed exchange in ^{18}O-water to produce $-{}^{13}C^{18}O^{18}OH$ groups and *in situ* silylation to produce Fmoc-protected residues for solid-phase protein synthesis. An isotopic purity of ≥90% was confirmed by ESI mass spectrometry. Isotopically labeled forms of Aβ40 were synthesized with $^{13}C{=}{=}^{18}O$ labels in residues G25*, G29*, G33*, G38*, and A21*, with the asterisk indicating the presence of one double label in each protein.

Sample Preparation. Lyophilized proteins were dissolved in 40% hexafluoroisopropanol with 5 mM HCl for 30 min to remove residual trifluoroacetic acid. The hexafluoroisopropanol was added to prevent Aβ40 aggregation. The proteins were then relyophilized, dissolved at a concentration of 200 μM in D_2O containing 10 mM DCl (pD = 2.0) and 0.04% sodium azide, and incubated at 37°C without any agitation. Under these conditions, fibrils formed slowly over the course of several weeks. At selected times, 5-μl aliquots of these solutions were placed on a CaF_2 window and allowed to evaporate, yielding films suitable for linear and 2D IR experiments. These aliquots produced films ≈7 mm in diameter, i.e., smaller than the 1-cm beam in the linear IR instrument but much larger than the 150-μm-diameter region probed in 2D IR experiments.

Linear IR. Spectra were collected in rapid-scanning mode as 1,024 coadded interferograms by using a Bio-Rad FTS-60A spectrometer, a liquid-nitrogen-cooled MCT detector, a resolution of 2 cm^{-1}, a scanning speed of 20 MHz, and an undersampling ratio of 2. The instrument was continuously purged with dry CO_2-free air. Spectra were processed with one level of zero filling and triangular apodization, but no smoothing, deconvolution, vapor subtraction, or non-level baseline correction.

The 2D IR. The 2D IR experimental schemes and data-processing procedures have been described in detail elsewhere (46). Briefly, three 400-nJ transform-limited 75-fs pulses having the same polarization and with wave vectors k_1, k_2, and k_3 at time interval τ between the first and second, and T between the second and third, were used to generate the photon echo in a phase-matched direction of $-k_1 + k_2 + k_3$. The signal and a heterodyning pulse preceding it by an interval of ≈700 fs were combined at the focal plane of a monochromator combined with a 64-element MCT array detector (IR Associates), enabling the signal to be measured as a function of detection time, t. The range of τ scanned was −3 to 4.5 ps in 2-fs steps, where negative and positive values represent nonrephasing and rephasing schemes, respectively. The IR pulses were centered at 1,600 cm^{-1} for all of the samples. All 2D IR spectra were collected at 22°C and represent the real part of the absorptive (correlation) spectra. The 2D spectra are displayed as the double Fourier transforms of the (τ, t) data set with frequency arguments (ω_τ, ω_t).

Electron Microscopy. For EM details see *SI Materials and Methods: Electron Microscopy* and SI Figs. S1 and S2.

ACKNOWLEDGMENTS. We thank Dr. Ray Meade (Biochemical Imaging Core Facility of the University of Pennsylvania) for assistance with the EM and Dr. Igor Rubtsov (Tulane University, New Orleans, LA) for discussion. The research was supported by National Institutes of Health Grants GM76201 (to P.H.A.), GM12592 (to R.M.H.), and GM 48310 (to R.M.H.), a Zenith Fellows Award from the Alzheimer's Association (to P.H.A.), and instrumentation from National Institutes of Health Grant PO1RR01348.

1. Eanes ED, Glenner GG (1968) X-ray diffraction studies on amyloid filaments. *J Histochem Cytochem* 16:673–677.
2. Kirschner DA, *et al.* (1987) Synthetic peptide homologous to beta protein from Alzheimer disease forms amyloid-like fibrils in vitro. *Proc Natl Acad Sci USA* 84:6953–6957.
3. Sunde M, *et al.* (1997) Common core structure of amyloid fibrils by synchrotron x-ray diffraction. *J Mol Biol* 273:729–739.
4. Antzutkin ON, *et al.* (2000) Multiple quantum solid-state NMR indicates a parallel, not antiparallel, organization of β-sheets in Alzheimer's β-amyloid fibrils. *Proc Natl Acad Sci USA* 97:13045–13050.
5. Torok M, *et al.* (2002) Structural and dynamic features of Alzheimer's Aβ peptide in amyloid fibrils studied by site-directed spin labeling. *J Biol Chem* 277:40810–40815.
6. Petkova AT, *et al.* (2002) A structural model for Alzheimer's β-amyloid fibrils based on experimental constraints from solid state NMR. *Proc Natl Acad Sci USA* 99:16742–16747.
7. Petkova AT, Yau W-M, Tycko R (2006) Experimental constraints on quaternary structure in Alzheimer's β-amyloid fibrils. *Biochemistry* 45:498–512.
8. Wetzel R, Shivaprasad S, Williams AD (2007) Plasticity of amyloid fibrils. *Biochemistry* 46:1–10.
9. Luhrs T, *et al.* (2005) 3D structure of Alzheimer's amyloid-β(1–42) fibrils. *Proc Natl Acad Sci USA* 102:17342–17347.
10. Hamm P, Lim M, Hochstrasser RM (1998) Structure of the amide I band of peptides measured by femtosecond nonlinear-infrared spectroscopy. *J Phys Chem B* 102:6123–6138.
11. Asplund MC, Zanni MT, Hochstrasser RM (2000) Two-dimensional infrared spectroscopy of peptides by phase-controlled femtosecond vibrational photon echoes. *Proc Natl Acad Sci USA* 97:8219–8224.
12. Hochstrasser RM (2007) Two-dimensional spectroscopy at infrared and optical frequencies. *Proc Natl Acad Sci USA* 104:14190–14196.
13. Fang C, *et al.* (2004) Two-dimensional infrared spectroscopy of isotopomers of an alanine rich α-helix. *J Phys Chem B* 108:10415–10427.
14. Cheatum CM, Tokmakoff A, Knoester J (2004) Signatures of β-sheet secondary structures in linear and two-dimensional infrared spectroscopy. *J Chem Phys* 120:8201–8215.
15. Hamm P, Lim M, DeGrado WF, Hochstrasser RM (1999) The two-dimensional IR nonlinear spectroscopy of a cyclic penta-peptide in relation to its three-dimensional structure. *Proc Natl Acad Sci USA* 96:2036–2041.
16. Kim YS, Hochstrasser RM (2007) Observation of kinetic networks of hydrogen-bond exchange using 2D IR echo spectroscopy. *Springer Series Chem Phys* 88:332–334.
17. Londergan CH, Wang J, Axelsen PH, Hochstrasser RM (2006) Two-dimensional infrared spectroscopy displays signatures of structural ordering in peptide aggregates. *Biophys J* 90:4672–4685.
18. Chung HS, Ganim Z, Jones KC, Tokmakoff A (2007) Transient two-dimensional IR spectroscopy of ubiquitin unfolding dynamics. *Proc Natl Acad Sci USA* 104:14237–14242.
19. Zhuang W, Abramavicius D, Voronine DV, Mukamel S (2007) Simulation of two-dimensional infrared spectroscopy of amyloid fibrils. *Proc Natl Acad Sci USA* 104:14233–14236.
20. Shim S-H, Strasfeld DB, Ling YL, Zanni MT (2007) Automated two-dimensional IR spectroscopy using a mid-IR pulse shaper and application of this technology to the human islet amyloid polypeptide. *Proc Natl Acad Sci USA* 104:14197–14202.
21. Hochstrasser RM, Whiteman JD (1972) Exciton band structure and properties of a real linear chain in a molecular crystal. *J Chem Phys* 56:5945–5958.
22. Abramavicius D, Zhuang W, Mukamel S (2004) Peptide secondary structure determination by three-pulse coherent vibrational spectroscopies: A simulation study. *J Phys Chem B* 108:18034–18045.
23. Bandekar J, Krimm S (1988) Vibrational analysis of peptides, polypeptides, and proteins. 39. Normal mode spectrum of the parallel-chain β-sheet. *Biopolymers* 27:909–921.
24. Bour P, Keiderling TA (2004) Structure, spectra and the effects of twisting of β-sheet peptides. A density functional theory study. *Theochem* 675:95–105.
25. Paul C, Wang J, Wimley WC, Hochstrasser RM, Axelsen PH (2004) Vibrational coupling, isotopic editing, and β-sheet structure in a membrane-bound polypeptide. *J Am Chem Soc* 126:5843–5850.
26. Schreiber M, Toyozawa Y (1982) Numerical experiments on the absorption lineshape of the exciton under lattice vibrations. II. The average oscillator strength per state. *J Phys Soc Jpn* 51:1537–1543.
27. Blumen A, Lemaistre JP, Mathlouthi I (1984) Localization of exciton states in structurally disordered materials. *J Chem Phys* 81:4610–4613.
28. Wang J, Hochstrasser RM (2004) Characteristics of the two-dimensional infrared spectroscopy of helices from approximate simulations and analytic models. *Chem Phys* 297:195–219.
29. Bednarz M, Malyshev VA, Knoester J (2004) Low-temperature dynamics of weakly localized Frenkel excitons in disordered linear chains. *J Chem Phys* 120:3827–3840.
30. Merz PA, *et al.* (1983) Ultrastructural morphology of amyloid fibrils from neuritic and amyloid plaques. *Acta Neuropathol* 60:113–124.
31. Narang HK (1980) High-resolution electron microscopic analysis of the amyloid fibril in Alzheimer's disease. *J Neuropathol Exp Neurol* 39:621–631.
32. Koppaka V, Paul C, Murray IV, Axelsen PH (2003) Early synergy between Aβ42 and oxidatively damaged membranes in promoting amyloid fibril formation by Aβ40. *J Biol Chem* 278:36277–36284.
33. Paul C, Axelsen PH (2005) β sheet structure in amyloid β fibrils and vibrational dipolar coupling. *J Am Chem Soc* 127:5754–5755.
34. Choi J-H, Ham S, Cho M (2003) Local amide I mode frequencies and coupling constants in polypeptides. *J Phys Chem B* 107:9132–9138.
35. Agranovich VM, Kamchatnov AM (1999) Quantum confinement and superradiance of one-dimensional self-trapped Frenkel excitons. *Chem Phys* 245:175–184.
36. Fidder H, Knoester J, Wiersma DA (1991) Optical properties of disordered molecular aggregates: A numerical study. *J Chem Phys* 95:7880–7890.
37. Mukamel S (1995) *Principles of Nonlinear Optical Spectroscopy* (Oxford Univ Press, New York).
38. Torii H, Tasumi M (1992) Model calculations on the amide-I infrared bands of globular proteins. *J Chem Phys* 96:3379–3387.
39. Balbach JJ, *et al.* (2002) Supramolecular structure in full-length Alzheimer's β-amyloid fibrils: Evidence for a parallel β-sheet organization from solid-state nuclear magnetic resonance. *Biophys J* 83:1205–1216.
40. la Cour Jansen T, Knoester J (2006) A transferable electrostatic map for solvation effects on amide I vibrations and its application to linear and two-dimensional spectroscopy. *J Chem Phys* 124:044502/1–044502/11.
41. Ham S, Kim J-H, Lee H, Cho M (2003) Correlation between electronic and molecular structure distortions and vibrational properties. II. Amide I modes of NMA-nD2O complexes. *J Chem Phys* 118:3491–3498.
42. Hayashi T, Zhuang W, Mukamel S (2005) Electrostatic DFT map for the complete vibrational amide band of NMA. *J Phys Chem A* 109:9747–9759.
43. Schmidt JR, Corcelli SA, Skinner JL (2004) Ultrafast vibrational spectroscopy of water and aqueous N-methylacetamide: Comparison of different electronic structure/molecular dynamics approaches. *J Chem Phys* 121:8887–8896.
44. Wang J, Zhuang W, Mukamel S, Hochstrasser R (2008) Two-dimensional infrared spectroscopy as a probe of the solvent electrostatic field for a twelve residue peptide. *J Phys Chem B* 112:5930–5937.
45. Baker NA, Sept D, Joseph S, Holst MJ, McCammon JA (2001) Electrostatics of nanosystems: Application to microtubules and the ribosome. *Proc Natl Acad Sci USA* 98:10037–10041.
46. Kim YS, Wang J, Hochstrasser RM (2005) Two-dimensional infrared spectroscopy of the alanine dipeptide in aqueous solution. *J Phys Chem B* 109:7511–7521.